Eur. Phys. J. C (2015) 75:416
DOI 10.1140/epjc/s10052-015-3627-y

THE EUROPEAN PHYSICAL JOURNAL C

Regular Article - Experimental Physics

Results on $\beta\beta$ decay with emission of two neutrinos or Majorons in ^{76}Ge from GERDA Phase I

GERDA Collaboration[1,a]

M. Agostini[16], **M. Allardt**[5], **A. M. Bakalyarov**[14], **M. Balata**[2], **I. Barabanov**[12], **N. Barros**[5,21], **L. Baudis**[20], **C. Bauer**[8], **N. Becerici-Schmidt**[15], **E. Bellotti**[9,10], **S. Belogurov**[12,13], **S. T. Belyaev**[14], **G. Benato**[20], **A. Bettini**[17,18], **L. Bezrukov**[12], **T. Bode**[16], **D. Borowicz**[4,6], **V. Brudanin**[6], **R. Brugnera**[17,18], **D. Budjáš**[16], **A. Caldwell**[15], **C. Cattadori**[10], **A. Chernogorov**[13], **V. D'Andrea**[2], **E. V. Demidova**[13], **A. di Vacri**[2], **A. Domula**[5], **E. Doroshkevich**[12], **V. Egorov**[6], **R. Falkenstein**[19], **O. Fedorova**[12], **K. Freund**[19], **N. Frodyma**[4], **A. Gangapshev**[8,12], **A. Garfagnini**[17,18], **P. Grabmayr**[19], **V. Gurentsov**[12], **K. Gusev**[6,14,16], **A. Hegai**[19], **M. Heisel**[8], **S. Hemmer**[17,18], **G. Heusser**[8], **W. Hofmann**[8], **M. Hult**[7], **L. V. Inzhechik**[12,22], **J. Janicskó Csáthy**[16], **J. Jochum**[19], **M. Junker**[2], **V. Kazalov**[12], **T. Kihm**[8], **I. V. Kirpichnikov**[13], **A. Kirsch**[8], **A. Klimenko**[6,8,23], **K. T. Knöpfle**[8], **O. Kochetov**[6], **V. N. Kornoukhov**[12,13], **V. V. Kuzminov**[12], **M. Laubenstein**[2], **A. Lazzaro**[16], **V. I. Lebedev**[14], **B. Lehnert**[5], **H. Y. Liao**[15], **M. Lindner**[8], **I. Lippi**[18], **A. Lubashevskiy**[6,8], **B. Lubsandorzhiev**[12], **G. Lutter**[7], **C. Macolino**[2], **B. Majorovits**[15], **W. Maneschg**[8], **E. Medinaceli**[17,18], **M. Misiaszek**[4], **P. Moseev**[12], **I. Nemchenok**[6], **D. Palioselitis**[15], **K. Panas**[4], **L. Pandola**[3], **K. Pelczar**[4], **A. Pullia**[11], **S. Riboldi**[11], **N. Rumyantseva**[6], **C. Sada**[17,18], **M. Salathe**[8], **C. Schmitt**[19], **B. Schneider**[5], **S. Schönert**[16], **J. Schreiner**[8], **A.-K. Schütz**[19], **O. Schulz**[15], **B. Schwingenheuer**[8], **O. Selivanenko**[12], **M. Shirchenko**[6,14], **H. Simgen**[8], **A. Smolnikov**[8], **L. Stanco**[18], **M. Stepaniuk**[8], **C. A. Ur**[18], **L. Vanhoefer**[15], **A. A. Vasenko**[13], **A. Veresnikova**[12], **K. von Sturm**[17,18], **V. Wagner**[8], **M. Walter**[20], **A. Wegmann**[8], **T. Wester**[5], **H. Wilsenach**[5], **M. Wojcik**[4], **E. Yanovich**[12], **P. Zavarise**[2], **I. Zhitnikov**[6], **S. V. Zhukov**[14], **D. Zinatulina**[6], **K. Zuber**[5], **G. Zuzel**[4]

[1] LNGS, Assergi, Italy
[2] INFN Laboratori Nazionali del Gran Sasso and Gran Sasso Science Institute, Assergi, Italy
[3] INFN Laboratori Nazionali del Sud, Catania, Italy
[4] Institute of Physics, Jagiellonian University, Cracow, Poland
[5] Institut für Kern- und Teilchenphysik, Technische Universität Dresden, Dresden, Germany
[6] Joint Institute for Nuclear Research, Dubna, Russia
[7] Institute for Reference Materials and Measurements, Geel, Belgium
[8] Max-Planck-Institut für Kernphysik, Heidelberg, Germany
[9] Dipartimento di Fisica, Università Milano Bicocca, Milan, Italy
[10] INFN Milano Bicocca, Milan, Italy
[11] Dipartimento di Fisica, Università degli Studi di Milano e INFN Milano, Milan, Italy
[12] Institute for Nuclear Research of the Russian Academy of Sciences, Moscow, Russia
[13] Institute for Theoretical and Experimental Physics, Moscow, Russia
[14] National Research Centre "Kurchatov Institute", Moscow, Russia
[15] Max-Planck-Institut für Physik, Munich, Germany
[16] Physik Department and Excellence Cluster Universe, Technische Universität München, Munich, Germany
[17] Dipartimento di Fisica e Astronomia dell'Università di Padova, Padua, Italy
[18] INFN Padova, Padua, Italy
[19] Physikalisches Institut, Eberhard Karls Universität Tübingen, Tübingen, Germany
[20] Physik Institut der Universität Zürich, Zurich, Switzerland
[21] *Present Address:* Department of Physics and Astronomy, University of Pennsylvania, Philadelphia, PA, USA
[22] *Also at:* Moscow Institute of Physics and Technology, Moscow, Russia
[23] *Also at:* International University for Nature, Society and Man "Dubna", Dubna, Russia

Received: 9 January 2015 / Accepted: 18 August 2015 / Published online: 9 September 2015
© The Author(s) 2015. This article is published with open access at Springerlink.com

Abstract A search for neutrinoless $\beta\beta$ decay processes accompanied with Majoron emission has been performed using data collected during Phase I of the GERmanium Detector Array (GERDA) experiment at the Laboratori Nazionali del Gran Sasso of INFN (Italy). Processes with

[a] e-mail: gerda-eb@mpi-hd.mpg.de

spectral indices $n = 1, 2, 3, 7$ were searched for. No signals were found and lower limits of the order of 10^{23} yr on their half-lives were derived, yielding substantially improved results compared to previous experiments with ^{76}Ge. A new result for the half-life of the neutrino-accompanied $\beta\beta$ decay of ^{76}Ge with significantly reduced uncertainties is also given, resulting in $T^{2\nu}_{1/2} = (1.926 \pm 0.094) \times 10^{21}$ yr.

1 Introduction

Neutrinoless double beta ($0\nu\beta\beta$) decay is regarded as the gold-plated process for probing the fundamental character of neutrinos. Observation of this process would imply total lepton number violation by two units and that neutrinos have a Majorana mass component. Although the main focus of the experimental efforts lies on the detection of $0\nu\beta\beta$ decay mediated by light Majorana neutrino exchange, there are also many other proposed mechanisms which are being searched for. Some exotic models predict $0\nu\beta\beta$ decays proceeding through the emission of a massless Goldstone boson, called Majoron. Predictions of different models depend on its transformation properties under weak isospin, singlet [1], doublet [2] and triplet [3]. Precise measurements of the invisible width of the Z boson at LEP [4] greatly disfavor triplet and pure doublet models. Several new Majoron models have been developed subsequently in which the Majoron carries leptonic charge and cannot be a Goldstone boson [5,6] or in which the $0\nu\beta\beta$ decay proceeds through the emission of two Majorons [7].

All these models predict different shapes of the two emitted electrons' summed energy spectrum. The predicted spectral shapes are essentially defined by the phase space of the emitted particles:

$$\frac{\mathrm{d}N}{\mathrm{d}K} \sim G \sim (Q_{\beta\beta} - K)^n \tag{1}$$

where K is the summed energy of the two electrons, G is the phase space, $Q_{\beta\beta}$ is the Q value of the $0\nu\beta\beta$ decay, and n is the spectral index of the model. Single Majoron-emitting $\beta\beta$ decays can be roughly divided into three classes, $n = 1$, $n = 2$, and $n = 3$. Double Majoron emitting decays can have either $n = 3$ or $n = 7$. Their characteristic spectral shapes differ from that of two-neutrino $\beta\beta$ decay ($2\nu\beta\beta$), for which $n = 5$. This allows for discrimination between the processes.

Experimental searches for $\beta\beta$ decay mediated by emission of one or two Majorons ($0\nu\beta\beta\chi$) have been performed by the Heidelberg-Moscow experiment (HDM) for ^{76}Ge [8,9]; by NEMO-2 and NEMO-3 for ^{100}Mo, ^{116}Cd, ^{82}Se, ^{96}Zr, ^{130}Te [10–15]; by ELEGANT V for ^{100}Mo [16]; by DAMA [17], KAMLAND-Zen [18] and EXO-200 [19] for ^{136}Xe. None of these experiments have seen an excess of events that could be interpreted as a Majoron signal; they reported lower limits on the half-lives of the processes that involve Majoron emission.

The $2\nu\beta\beta$ decay process conserves lepton number and is independent of the nature of the neutrino. It has been detected for 11 nuclides so far, with measured half-lives ($T^{2\nu}_{1/2}$) in the range of 7×10^{18}–2×10^{24} yr [20–24]. The knowledge of $T^{2\nu}_{1/2}$ allows for extraction of the nuclear matrix element, $\mathcal{M}^{2\nu}$, which can provide some constraints on that of $0\nu\beta\beta$ decay, $\mathcal{M}^{0\nu}$, if the evaluations of $\mathcal{M}$ for the two processes are performed within the same model [25–32].

This paper reports on the search for neutrinoless double beta decay of ^{76}Ge with Majoron emission ($0\nu\beta\beta\chi$) and a new analysis of the half-life of the $2\nu\beta\beta$ decay of ^{76}Ge using data collected by the GERmanium Detector Array (GERDA) experiment during its Phase I. $2\nu\beta\beta$ decay is a well established and previously observed process, while $0\nu\beta\beta\chi$ decay is a hypothetical one. In the first case the half-life is extracted, while for the second one a limit is set. This leads to slightly different approaches in the analyses leading to different data sets and background components being used.

2 The GERDA experiment

The main aim of the GERDA experiment [33] at the Laboratori Nazionali del Gran Sasso (LNGS) of INFN in Italy is to search for $0\nu\beta\beta$ decay of ^{76}Ge. The core of the setup is an array of high-purity germanium (HPGe) detectors made from isotopically modified material with ^{76}Ge enriched to ~86 % ($^{\mathrm{enr}}$Ge), mounted in low-mass copper supports (holders) and immersed in a 64 m^3 cryostat filled with liquid argon (LAr). The LAr serves as cooling medium and shield against external backgrounds. The shielding is complemented by water in a tank of 10 m in diameter which is instrumented with photomultipliers to detect Cherenkov light generated in muon-induced showers [33].

The array of HPGe detectors is arranged in strings. Each string is enclosed with a cylinder, made from 60 μm thick Cu foil, called mini-shroud, to mitigate the background coming from the decay of ^{42}Ar present in the LAr. Moreover, in order to prevent contamination from radon within the cryostat, a cylinder, made from 30 μm thick Cu foil, called radon-shroud, separates the central part of the cryostat, where the detectors are located, from the rest. The HPGe detector signals are read out with custom-made charge sensitive preamplifiers optimized for low radioactivity, which are operated close to the detectors in the LAr. The analog signals are digitized with 100 MHz Flash ADCs (FADC) and analyzed offline. If one of the detectors has an energy deposition above the trigger threshold (40–100 keV), all channels are read out. Reprocessed p-type coaxial detectors from the HDM [34] and IGEX [35] experiments were operated together with Broad

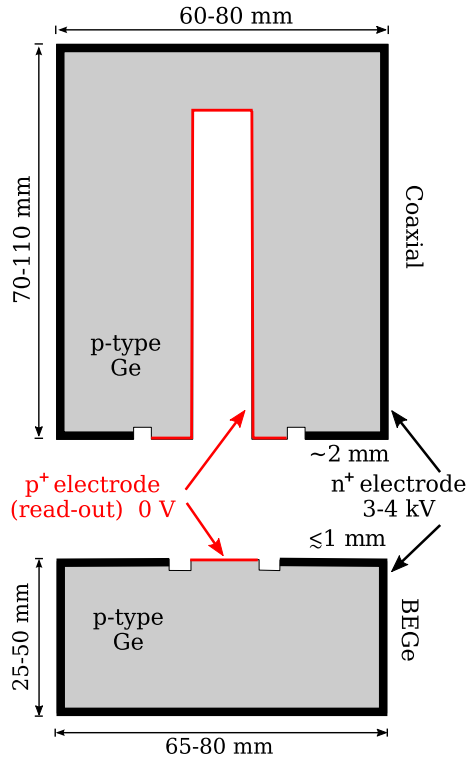

Fig. 1 Schematic sketch of a coaxial HPGe detector (*top*) and a BEGe detector (*bottom*) with their different surfaces and dead layers (drawings not to scale), adapted from Ref. [38]

Energy Germanium (BEGe) type detectors manufactured by Canberra [36,37].

As explained in Sect. 5, some background components have different effects on the two detector types due to their peculiar geometry. A schematic drawing of a coaxial detector type is shown in the top part of Fig. 1, while the lower part depicts that for a BEGe type detector.

3 Data taking and data selection

Phase I data taking lasted from November 9, 2011, to May 21, 2013. The total exposure collected comprises 19.2 kg yr for the coaxial detectors and 2.4 kg yr for the BEGe detectors. In this paper, the entire exposure collected by the BEGe detectors (BEGe data set) and 17.9 kg yr from the coaxial detectors (golden data set) are used [38,39]. For the coaxial detectors, a data set collected for 1.3 kg yr exposure during a restricted time period around the deployment of the BEGe detectors is discarded due to a higher background level. Also one of the coaxial detectors, RG2, is not considered for the data analysis starting from March 2013, as its high voltage had to be reduced below depletion voltage due to increased leakage current. The energy calibration of the detectors was performed using the information from dedicated calibration runs. For these calibration runs, three ^{228}Th sources were lowered to the vicinity of the detectors. The stability of the energy scale was monitored by performing such calibration runs every 1 or 2 weeks. Moreover, the stability of the system was continuously monitored by injecting charge pulses into the test input of the preamplifiers. Using physics data, the interpolated FWHM values at $Q_{\beta\beta}$ averaged with the exposure are (4.8 ± 0.2) keV for the coaxial detectors and (3.2 ± 0.2) keV for the BEGe detectors.

All steps of the offline processing of the GERDA data were performed within the software framework GELATIO [40]. The energy deposited in each detector was extracted from the respective charge pulse by applying an approximate Gaussian filter [41]. Non-physical events, such as discharges, cross-talk and pick-up noise events, were rejected by quality cuts based on the time position of the rising edge, the information from the Gaussian filter, the rise time and the charge pulse height, which must not exceed the dynamic range of the FADCs. Pile-up and accidental coincidences were removed from the data set using cuts based on the baseline slope (which should be compatible with zero for normal events), the number of triggers in a 10 μs time window and the position of the main rising edge. The rate of pile-up and accidental coincidence events is negligible in the GERDA data due to the extremely low event rate. The loss due to mis-classification by the quality cuts was <0.1 % for events with energies above 1 MeV. All events that come within 8 μs of a signal from the muon veto were rejected. Finally, only events that survive the detector anti-coincidence cut were considered. This means that all events with an energy deposition >50 keV in more than one detector in the array were not taken into account. Since $2\nu\beta\beta$ and $0\nu\beta\beta\chi$ events release their energy within a small volume inside the detectors, almost no signal events were lost by this cut, while a part of the γ-induced background events were rejected. The high efficiency of the anti-coincidence cut was checked using Monte Carlo generated events: the loss of $2\nu\beta\beta$ and $0\nu\beta\beta\chi$ events was estimated to be 0.14 % for energies above 570 keV.

4 Analysis strategy

The two analyses described in this paper are different in the sense that for $2\nu\beta\beta$ decay a parameter is extracted for a well established and known process, while in the case of the search for $0\nu\beta\beta\chi$ decay limits for a hypothetical process are set. In order to minimize the systematic uncertainties for the extraction of $T^{2\nu}_{1/2}$ a well defined and controlled subset of the data is used. Only unambiguously identified background processes are taken into account. For $0\nu\beta\beta\chi$ limit setting the exposure is maximized and all known possible background processes that cannot be unambiguously detected but could mimic $0\nu\beta\beta\chi$ decay are taken into account as otherwise a fake signal could be produced.

For the $T_{1/2}^{2\nu}$ analysis the golden data set (17.9 kg yr) with the coaxial detectors is used in order to have a large data sample obtained in well controlled experimental conditions. The Majoron analysis uses both the golden data set and the BEGe data set for a total exposure of 20.3 kg yr in order to maximize the sensitivity.

The background model for the $T_{1/2}^{2\nu}$ analysis uses a minimal number of components, assuming all sources close to the detectors [38,42]. Contributions from possible other sources are summarized in the systematic uncertainty. For the Majoron analysis, an expanded model is used [43], taking into account also additional medium and far distant positions for some of the sources.

In both analyses, the experimental spectra of the coaxial and BEGe detectors are analyzed using the Bayesian Analysis Toolkit (BAT) [44].

5 The background model

The background sources considered in the models were identified by their prominent structures in the energy spectra and were also expected on the basis of material screening measurements. The spectral shapes of individual background contributions were obtained by using a detailed implementation of the experimental setup in the Monte Carlo (MC) simulation framework MaGe [45]. A Bayesian spectral fit of the measured energy spectrum with the simulated spectra was performed in an energy range from 570 keV up to the end of the dynamic range at 7500 keV. The low energy limit is motivated by the β decay of ^{39}Ar, which gives a large contribution up to its Q_β-value of 565 keV. The high energy limit is dictated by the contamination coming from isotopes in the ^{226}Ra decay chain. Events from these decays reach into the energy region of interest of the present two analyses. More details can be found in Ref. [38].

The following background components were used for the extraction of $T_{1/2}^{2\nu}$ (minimum model in Refs. [38,42]): (1) ^{76}Ge $2\nu\beta\beta$ decay, (2) ^{214}Bi, ^{228}Ac, ^{228}Th, ^{60}Co and ^{40}K decays in the close vicinity of the detectors (<2 cm, represented by decays in the detector holders in the MC simulation), (3) decays of ^{60}Co inside the detectors, constrained by the maximum expected activity from their cosmogenic activation history, (4) ^{42}K decays in LAr assuming a uniform distribution, (5) α model that accounts for α decays originating from ^{210}Po and ^{226}Ra contaminations on the p^+ surface of the detectors as well as from ^{222}Rn in the LAr, and finally (6) ^{214}Bi decays on the p^+ surface, constrained by the estimated ^{226}Ra activity from the α model.

The parameters of all components besides the constrained ones were given a flat prior probability distribution. There are no strong correlations between the model parameters since all considered background components have characteristic features such as γ-ray lines or peak-like structures at different energies. The ratios of the γ-ray line intensities from the individual considered background sources suggest contaminations dominantly in locations close to the detectors. Hence, the minimum model takes into account only the close-by source locations. Nevertheless, the screening measurements indicate contaminations of materials in farther locations as well. An additional contribution can come from ^{42}K decays at or near the detector n^+ surfaces (see Fig. 1) with a specific activity higher than that for the uniform distribution assumption. This component is the dominating one for the BEGe data set, as the thinner dead layer thickness of BEGes of roughly 1 mm allows penetration of the electrons emitted in the decay of ^{42}K to the active volume, while for coaxial detectors the dead layer thickness of $\sim$2 mm efficiently shields this background component.

The spectral shapes of the contributions from the background sources without significant multiple γ peaks at different source locations differ only marginally. This makes it impossible to pinpoint the exact source locations given the available statistics of the measured spectra. Note that adding all well motivated but not unambiguously identified background contributions does not influence the best-fit value for $T_{1/2}^{2\nu}$ significantly (see Table 8 in Ref. [38]). Variations of individual source locations for the considered decays were taken into account when evaluating the systematic uncertainty of $T_{1/2}^{2\nu}$ as described in Sect. 7.2.

For the Majoron analysis additional background components were used [43], including also medium and far distant contributions. For the coaxial detectors ^{42}K on the n^+ and on the p^+ contacts was added to the list of the close sources of the previous background model. For medium distances, i.e. between 2 and 50 cm from the detectors, contributions from the following sources were added: ^{214}Bi, ^{228}Th and ^{228}Ac. A ^{228}Th contamination was chosen as a representative for far distant sources (above 50 cm). Whenever possible, screening measurements were used to constrain the lower limit of the expected background events.

In the Majoron analysis, also the data collected with the BEGe diodes were used in order to maximize the exposure. Consequently, the background model developed for these detectors was used [38,43]. The same close, medium, and far distant sources as for the coaxial detectors were used. ^{68}Ge was added as internal source. This was necessary in order to take into account the cosmic activation of the germanium due to the recent production of these diodes. The most probable backgrounds have been quoted in Tables 6 and 9 of Ref. [38].

6 Determination of the half-life of $2\nu\beta\beta$ decay

6.1 Analysis

The $T_{1/2}^{2\nu}$ of $2\nu\beta\beta$ decay of ^{76}Ge was determined considering the golden data set of Phase I, amounting to an exposure of

17.9 kg yr, and using the background model prediction for the contribution of the $2\nu\beta\beta$ spectrum to the overall energy spectrum. Details of the background analysis can be found in Ref. [42].

The global fit for the background modeling was performed on the summed energy spectrum of the coaxial detectors using a bin width of 30 keV. Thus, the scaling parameter of the $2\nu\beta\beta$ spectrum in the model, $N_{2\nu}^{\text{fit}}$, gives the number of events in the $2\nu\beta\beta$ spectrum in the fit window of 570–7500 keV for all detectors. Using this result for the number of measured $2\nu\beta\beta$ events, the half-life is calculated as

$$T_{1/2}^{2\nu} = \frac{(\ln 2)\ N_{\text{A}}}{m_{\text{enr}}\ N_{2\nu}^{\text{fit}}} \sum_{i=1}^{N_{\text{det}}} M_i\ t_i\ f_{76,i}[f_{\text{AV},i}\ \varepsilon_{\text{AV},i}^{\text{fit}} + (1 - f_{\text{AV},i})\ \varepsilon_{\text{DL},i}^{\text{fit}}], \quad (2)$$

where N_{A} is Avogadro's constant and $m_{\text{enr}} = 75.6$ g is the molar mass of the enriched material. The summation runs over all the detectors (N_{det}) considered in the data set. All detector related parameters like the detector mass (M_i), the time of the data taking for each detector (t_i), the fraction of ^{76}Ge atoms ($f_{76,i}$), the active volume fraction ($f_{\text{AV},i}$), and the detection efficiencies in the active volume ($\varepsilon_{\text{AV},i}^{\text{fit}}$) and in the dead layer ($\varepsilon_{\text{DL},i}^{\text{fit}}$) are taken into account separately for the individual detectors. All values are listed in Table 1. The efficiency $\varepsilon_{\text{AV},i}^{\text{fit}}$ ($\varepsilon_{\text{DL},i}^{\text{fit}}$) corresponds to the probability that a $2\nu\beta\beta$ decay taking place in the active volume (dead layer) of the detector deposits detectable energy in the fit window considered for the background model. The detection efficiencies, on average $\varepsilon_{\text{AV}}^{\text{fit}} = 0.667$ and $\varepsilon_{\text{DL}}^{\text{fit}} = 0.011$, are obtained through dedicated MC simulations. The statistical uncertainty due to the number of simulated events is on the order of 0.1 %.

The background model resulted in a scaling parameter of $N_{2\nu}^{\text{fit}} = 25690\ ^{+310}_{-330}$ for the $2\nu\beta\beta$ spectrum, which is the best-fit parameter. The uncertainty is given by the smallest 68 % probability interval of the marginalized posterior probability distribution. Using this result, the half-life derived according to Eq. 2 is

$$T_{1/2}^{2\nu} = (1.926\ ^{+0.025}_{-0.022}) \times 10^{21}\ \text{yr}. \quad (3)$$

6.2 Systematic uncertainties

The systematic uncertainties affecting the result for $T_{1/2}^{2\nu}$ were grouped into the three categories (i) *detector parameters and fit model*, (ii) *MC simulation*, and (iii) *data acquisition and selection*. The contributions to the total systematic uncertainty on $T_{1/2}^{2\nu}$ are summarized in Table 2.

(i) *Detector parameters and fit model*

– The systematic uncertainty on the active ^{76}Ge exposure ($\mathcal{E}_{\text{AV},76}$) was determined using a MC approach. $\mathcal{E}_{\text{AV},76}$ is defined as

$$\mathcal{E}_{\text{AV},76} = \sum_{i=1}^{N_{\text{det}}} M_i t_i\, f_{\text{AV},i}\, f_{76,i}. \quad (4)$$

For evaluating its uncertainty, the parameters of the individual detectors were randomly sampled from Gaussian distributions with mean values and standard deviations according to the corresponding values listed in Table 1. The correlated terms for f_{AV} were also taken into account. The live time t is calculated using the monitoring test pulses, which had a rate of 0.1 Hz in a first period of the data taking and

Table 1 Parameters for the coaxial detectors (upper part) and for the BEGe detectors (lower part): live time, t, total mass, M, the fraction of ^{76}Ge atoms, f_{76}, and the active volume fraction, f_{AV}. For the coaxial detectors, the first uncertainty on f_{act} is the uncorrelated part, the second one the correlated contribution. The values for M, f_{76}, and f_{AV} are taken from Ref. [38]

Detectors	t (days)	M (kg)	f_{76} (%)	f_{AV} (%)
Enriched coaxial detectors				
ANG2	485.5	2.833	86.6 ± 2.5	$87.1 \pm 4.3 \pm 2.8$
ANG3	485.5	2.391	88.3 ± 2.6	$86.6 \pm 4.9 \pm 2.8$
ANG4	485.5	2.372	86.3 ± 1.3	$90.1 \pm 4.9 \pm 2.9$
ANG5	485.5	2.746	85.6 ± 1.3	$83.1 \pm 4.0 \pm 2.7$
RG1	485.5	2.110	85.5 ± 1.5	$90.4 \pm 5.2 \pm 2.9$
RG2	384.8	2.166	85.5 ± 1.5	$83.1 \pm 4.6 \pm 2.7$
Enriched BEGe detectors				
GD32B	280.0	0.717	87.7 ± 1.3	89.0 ± 2.7
GD32C	304.6	0.743	87.7 ± 1.3	91.1 ± 3.0
GD32D	282.7	0.723	87.7 ± 1.3	92.3 ± 2.6
GD35B	301.2	0.812	87.7 ± 1.3	91.4 ± 2.9

Table 2 Contributions to the systematic uncertainty on $T_{1/2}^{2\nu}$ taken into account in this work. The total systematic uncertainty is obtained by combining the individual contributions in quadrature

Item	Uncertainty on $T_{1/2}^{2\nu}$ (%)	
Active ^{76}Ge exposure	± 4	
Background model components	$^{+1.4}_{-1.2}$	
Shape of the $2\nu\beta\beta$ spectrum	<0.1	
Subtotal fit model		± 4.2
Precision of the Monte Carlo geometry model	± 1	
Accuracy of the Monte Carlo tracking	± 2	
Subtotal Monte Carlo simulation		± 2.2
Data acquisition and handling		<0.1
Total		± 4.7

0.05 Hz in the remaining part. The data files were written to disk every 2 h, thus the uncertainty on t is 0.3–0.5%. The total detector masses are known with good accuracy (uncertainty smaller than 0.1 %). The calculation yields $\mathcal{E}_{\mathrm{AV},76} = (13.45 \pm 0.54)$ kg yr. The uncertainty of 4 % is dominated by the uncertainties on f_{AV} [38], while f_{76} gives a smaller contribution. These uncertainties mainly affect the number of ^{76}Ge nuclei in the active volume of the detectors, with a relatively smaller impact on the detection efficiency for the background sources. The determination of f_{AV} and its uncertainty is based on the intercomparison of calibration data (taken with ^{60}Co and ^{241}Am sources) with simulated calibration of the same experimental setup.

– The reference background model used for determining $T^{2\nu}_{1/2}$ accounts only for the dominant source locations in the setup. The systematic uncertainty due to the choice of the background model components was evaluated by repeating the global fit with alternative models, i.e., individual possible background components are added to the reference model and varied maximally, however, retaining a reasonable fit. The model that accounts for ^{228}Th and ^{228}Ac contributions also in the radon-shroud instead of only in the holders results in a 1.4 % longer $T^{2\nu}_{1/2}$. The same increase occurs if ^{40}K in the radon-shroud is added to the model components. The model including the contribution from ^{214}Bi in the radon-shroud in addition to the p^+ surface and holders yields a 0.7 % longer $T^{2\nu}_{1/2}$. In all the cases mentioned above, the contribution from background in the $2\nu\beta\beta$ spectrum region increases, since the peak-to-Compton ratio of the γ-rays decreases for farther source locations leading to longer $T^{2\nu}_{1/2}$ estimates. Excluding contributions from very close source locations, like ^{214}Bi on the p^+ surface and ^{60}Co on the germanium, results in a smaller increase of the best $T^{2\nu}_{1/2}$ estimate. In this case, the contributions from these components are compensated by ^{214}Bi and ^{60}Co decays in the holders, respectively. Consequently, the source locations are moved further out with respect to the reference model. Consistently, the models that include additional contributions from close source locations yield a decrease in the $T^{2\nu}_{1/2}$ value, e.g. including ^{214}Bi in LAr close to the p^+ surface (-1.0 %) or ^{42}K on the n^+ (-1.2 %) and p^+ (-0.6 %) surfaces. Comparing alternative background models to the reference one, the deviations in the $T^{2\nu}_{1/2}$ result range between -1.2 and $+1.4$ %.
– For the standard fit, a bin width of 30 keV was used for the data and MC energy spectra. In order to take into account the systematic uncertainty related to binning effects, the fit was repeated twice using bin widths of 10 and 50 keV. The bin width of 10 keV was chosen in order to minimize as much as possible the bin size taking into account the energy resolution of ≈4.5 keV of the coaxial detectors and the necessity to have enough statistics in all bins. Above 50 keV, peak structures are washed out, leading to a deterioration of the fit. The deviations in the $T^{2\nu}_{1/2}$ result were well within the statistical uncertainties, confirming that the uncertainty due to the bin width is properly treated within the fits. No systematic uncertainty was attributed due to the bin width.
– The primary spectrum of the two electrons emitted in the $2\nu\beta\beta$ decay of ^{76}Ge, which was then fed into the MC simulation, was sampled according to the distribution given in Ref. [21] (with the Primakoff–Rosen approximation removed) implemented in DECAY0 [46]. The systematic uncertainty due to the assumed $2\nu\beta\beta$ spectral shape was evaluated by comparing the spectrum generated by DECAY0 to the one given in Ref. [47]. Considering the analysis window used for background modeling, the maximum deviation is 0.2 % and the total deviation of the integral in the analysis window is 0.1 %. When the fit with the background model is repeated using the spectrum of Ref. [47], the difference from the reference the $T^{2\nu}_{1/2}$ result is less than 0.1 %.
– A possible effect of a transition layer, where it is assumed that the n^+ dead layer on the detector surfaces is partially active, has been investigated [48,49]. The dead layer thickness for individual detectors assumed in MC simulations was given according to the listed values in Ref. [38]. The transition layer is modeled using two different assumptions: a linearly and an exponentially increasing charge collection efficiency in the dead layer. The systematic uncertainty on $T^{2\nu}_{1/2}$ due to the $2\nu\beta\beta$ spectrum simulated with the transition layer is found to be negligible.

(ii) *MC simulation*

The uncertainty related to the MC simulation arises from the precision of the experimental geometry model implemented in MAGE (1 %) and from the accuracy of particle tracking (2 %) performed by GEANT4 [50–54]. The uncertainty on the particle tracking was estimated as reported in Ref. [56], the precision on the geometry model was estimated by changing the modeled geometry in the code (dimensions, displacements, materials). The total MC simulation uncertainty was estimated to be 2.2 % by summing in quadrature the aforementioned contributions.

(iii) *Data acquisition and selection*
The trigger and reconstruction efficiencies for physical events are practically 100 % above 100 keV in GERDA. These efficiencies were checked sending signals from a pulse generator to each detector. The amplitude of the signals was decreased down to 150 keV: no pulser events were lost by the trigger, quality cuts and reconstruction process. This result translates into an efficiency better than 99.9 % above 150 keV. The performance of the quality cuts has been further cross checked by a visual analysis. The total uncertainty related to data acquisition and selection was estimated to be less than 0.1 %.
Summing in quadrature the uncertainties of the three groups gives a total systematic uncertainty of ±4.7 %.

6.3 Results and discussion

Figure 2 shows the experimental data together with the best fit model for the golden data set. The different components of the minimum background model are also reported. The model is able to reproduce the experimental data well, as shown in the lower panel of the figure by the residuals. The p-value of the fit extending from 570 to 7500 keV is 0.02.

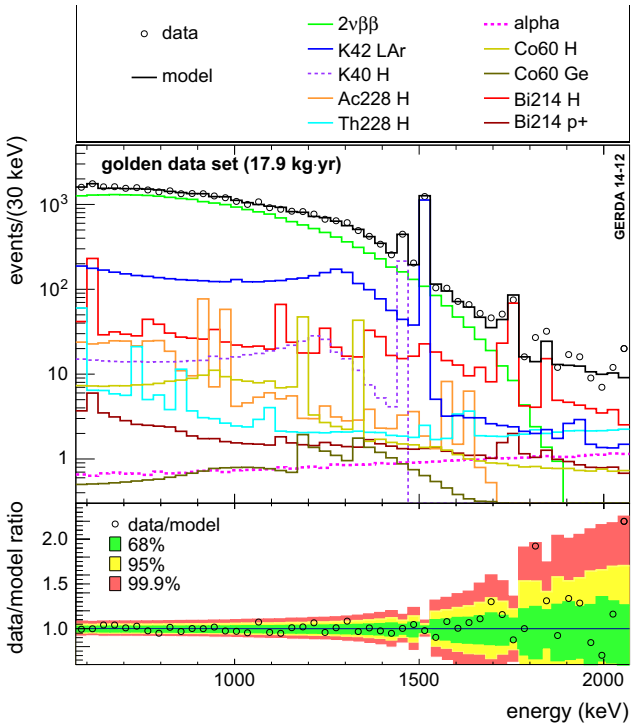

Fig. 2 *Upper panel*: experimental data (*markers*) and the best-fit model (*black histogram*) for the golden data set. The contributions from $2\nu\beta\beta$ (*green*) and from the single background components are also shown. *Lower panel*: ratio between experimental data and the prediction of the best-fit model. The *green*, *yellow*, and *red regions* are the smallest intervals containing 68, 95, and 99.9 % probability for the ratio assuming the best-fit parameters, respectively [55]

The best estimate of $T^{2\nu}_{1/2}$ of the $2\nu\beta\beta$ decay of ^{76}Ge is

$$T^{2\nu}_{1/2} = (1.926\,^{+0.025}_{-0.022\ \mathrm{stat}}\,^{+0.091}_{-0.091\ \mathrm{syst}}) \times 10^{21}\ \mathrm{yr} = (1.926 \pm 0.094) \times 10^{21}\ \mathrm{yr}, \quad (5)$$

with the latter combining in quadrature the statistical (fit) and systematic uncertainties. The total uncertainty of 4.9 % is dominated by the systematic uncertainties. The largest contribution to the systematic uncertainties comes from the uncertainty on the active ^{76}Ge exposure (4 %), which can only be reduced by performing new and more precise measurements of the active masses of the coaxial detectors. Other significant contributions are related to the Monte Carlo simulations (2.2 %) and to the background model assumptions ($^{+1.4\ \%}_{-1.2\ \%}$). The latter have been significantly reduced in this analysis compared to the analysis of the first 5 kg yr of Phase I data reported in Ref. [56], where the systematic uncertainty due to the background model was $^{+5.7\ \%}_{-2.1\ \%}$. The new result is in good agreement with that mentioned above. Adding further identified components to the reference background model results in a slight increase of the best $T^{2\nu}_{1/2}$ estimate.

The background level achieved in GERDA Phase I is about one order of magnitude lower with respect to predecessor ^{76}Ge experiments, and it has allowed the measurement of $T^{2\nu}_{1/2}$ with a signal-to-background ratio of 3:1 in the 570–2039 keV interval, or 4:1 in the smaller interval of 600–1800 keV. These ratios are much better than those for any past experiment that studied the $2\nu\beta\beta$ decay of ^{76}Ge.

7 Limits on Majoron-emitting double β decays of ^{76}Ge

7.1 Analysis

The search for $0\nu\beta\beta\chi$ decay was performed using the golden and BEGe data sets, amounting to a total exposure of 20.3 kg yr. The analysis employed the background model described in Sect. 5. The information from the two data sets was combined in one fit, while keeping their energy spectra distinct. A separate fit was performed for each spectral index, containing the background contributions, the contributions from $2\nu\beta\beta$ decay, and also the Majoron component under study. A single parameter, $T^{0\nu\chi}_{1/2}$, is considered common for the two data sets. It is defined as the half-life of the respective Majoron accompanied mode.

In order to improve the detection efficiency for the Majoron processes with low n ($n = 1, 2$), a slightly different event selection was used with respect to the $T^{2\nu}_{1/2}$ analysis. If an event occurs with energy deposition in two detectors and the energy deposit in the detector where the decay took place is below the threshold for the anti-coincidence cut, the event contributes to the energy spectrum of the other detector. Therefore, when determining the total energy spectrum

resulting from decays in one of the detectors, the energy spectra from all detectors in the array have to be taken into account. Such a selection has no impact on the detection efficiency for the Majoron process with $n = 3$ and 7 and $2\nu\beta\beta$ decay. The content of the ith bin in the combined energy spectrum of all N_{det} detectors in the array, for decays taking place in the active and dead part of detector α, becomes

$$\lambda_i^{\alpha,0\nu\chi} = \frac{(\ln 2)\ N_{\mathrm{A}}}{m_{\mathrm{enr}}\ T_{1/2}^{0\nu\chi}} M_\alpha\ f_{76,\alpha} \cdot \left[f_{\mathrm{AV},\alpha} \sum_{j=1}^{N_{\mathrm{det}}} t_j \varepsilon_{\mathrm{AV},j}^{\alpha} \Phi_{\mathrm{AV},i,j}^{\alpha,0\nu\chi} + (1 - f_{\mathrm{AV},\alpha}) \sum_{j=1}^{N_{\mathrm{det}}} t_j \varepsilon_{\mathrm{DL},j}^{\alpha} \Phi_{\mathrm{DL},i,j}^{\alpha,0\nu\chi} \right] \quad (6)$$

with $\Phi_{\mathrm{AV},i,j}^{\alpha,0\nu\chi}$ ($\Phi_{\mathrm{DL},i,j}^{\alpha,0\nu\chi}$) giving the content of the ith bin of the normalized energy distribution recorded with detector j for $0\nu\beta\beta\chi$ decay taking place in the active (dead) volume of detector α. Summing up the simulations of decays in all N_{det} detectors results in the final model spectrum:

$$\lambda_i^{0\nu\chi} = \sum_{\alpha=1}^{N_{\mathrm{det}}} \lambda_i^{\alpha,0\nu\chi}. \quad (7)$$

For all four Majoron modes ($n = 1, 2, 3, 7$) only lower limits on the half-life can be given because the interval of 68 % probability extends to infinite half-life. The limits were obtained from the 90 % quantiles of the marginalized posterior distributions. These lower limits for $T_{1/2}^{0\nu\chi}$, not taking into account the systematic uncertainties, are in units of 10^{23} yr: >4.4, >1.9, >0.9, and >0.4 for n = 1, 2, 3, and 7, respectively. The respective half-life of the $2\nu\beta\beta$ process derived from this analysis amounts to, in units of 10^{21} yr: $1.96 \pm 0.03_{\mathrm{stat}}$, $1.97 \pm 0.03_{\mathrm{stat}}$, $1.98 \pm 0.03_{\mathrm{stat}}$, and $1.99 \pm 0.03_{\mathrm{stat}}$. Within the uncertainties coming from the different background models and the different data sets of the two analyses, the derived $T_{1/2}^{2\nu}$ values are in agreement ($<1\sigma$) with that discussed in Sect. 6.3.

7.2 Systematic uncertainties

The systematic uncertainties were divided into the three categories (i) *detector parameters and fit model*, (ii) *MC simulation*, and (iii) *data acquisition and selection*.

(i) *Detector parameters and fit model*
Uncertainties from the fitting procedure were folded into the posterior distribution of $T_{1/2}^{0\nu\chi}$ with a MC approach. Each source of uncertainty is described by a probability distribution. The fitting procedure was repeated 1000 times, each time drawing a random number for each source of uncertainty according to its probability distribution:

- Material screening measurement results were used to constrain the minimum number of events expected from close and medium distant sources of the ^{214}Bi and ^{228}Th decays. Gaussian distributions describing these lower limits used in the fit were derived from the mean and standard deviations of the screening measurements. For details refer to Ref. [38].
- As for the $T_{1/2}^{2\nu}$ analysis, the standard fit uses a bin width of 30 keV for the data and MC energy spectra. In order to account for the systematic uncertainty related to binning effects the bin width was sampled uniformly from 10 to 50 keV.
- Uncertainties on the active volume fractions enter the model in several ways. On the one hand, the MC energy spectra for all internal sources, that is for $2\nu\beta\beta$, $0\nu\beta\beta\chi$, ^{60}Co, and ^{68}Ga decays, are affected, as the fraction of decays taking place in the active and dead part of the detectors changes with changing f_{AV}. On the other hand, the uncertainty on the active volume fraction also plays a role for the shape of the energy spectrum due to ^{42}K decays on the n^+ surface. Larger f_{AV} means thinner n^+ dead layer and thus the possibility of an increased contribution from the electrons to the spectrum. For smaller f_{AV} and thicker n^+ dead layer, their contributions are expected to be reduced. The active volume fraction for each detector was sampled from a Gaussian distribution with mean and standard deviation according to Table 1. For the coaxial detectors, the partial correlations of the uncertainty were taken into account. The simulated spectra of the internal sources as well as of the ^{42}K decays on the n^+ surface are composed according to the sampled active volume fractions.
- The uncertainty on the fraction of enrichment in ^{76}Ge of the germanium that constitutes the detectors plays a role when converting the number of events attributed to $0\nu\beta\beta\chi$ decay into $T_{1/2}^{0\nu\chi}$. The probability distribution of f_{76} for each detector is given by a Gaussian function with mean values and standard deviations as listed in Table 1.
- The data does not allow the resolution of the ambiguity regarding the exact positions of the near and medium distant sources. The ^{214}Bi decays serves as a representative in order to estimate the impact of this uncertainty. Their near position is represented by decays in the holders, in the mini-shroud or on the n^+ surface of the detectors, each having a probability of 1/3 in the sampling process. The medium distant position is represented by decays in the radon-shroud or in the LAr, having a probability 1/2 in contrast.
- Extensive studies of the characteristics of the BEGe diodes suggest the presence of a transition layer between the region where the detector is fully effi-

cient and the external dead region [48,49]. An uncertainty as high as ±0.5 % on the lower limits of $T_{1/2}^{0\nu\chi}$ is estimated for this effect in the case of the BEGe detectors. This uncertainty was folded into the total marginalized posterior distribution a posteriori. The corresponding uncertainty for the coaxial detectors is estimated to be negligible.

The marginalized posterior distributions for $T_{1/2}^{0\nu\chi}$ derived from each of the 1000 individual fits were summed up. The resulting total marginalized posterior distribution accounts for the statistical as well as for the listed systematic uncertainties related to the fit model. As for the $T_{1/2}^{2\nu}$ analysis, the uncertainties on the active volume fractions and on the enrichment fractions are major contributions to the total uncertainty on the limits for $T_{1/2}^{0\nu\chi}$. However, the largest source of uncertainty is the composition of the fit model and the individual background contributions. In the case of $n = 1$, a fit with a bin width of 50 keV weakens the limit by ≈16 % compared to the standard fit, while the result for $T_{1/2}^{2\nu}$ is not affected at all. The stability of the $T_{1/2}^{2\nu}$ results shows the validity of the fit. The use of the alternative close and medium distant source positions for ^{214}Bi decays leads to maximal variations of $^{+8.3}_{-12.6}$ % of the limit on $T_{1/2}^{0\nu\chi}$.

(ii) *MC simulation*
As in the case of the $T_{1/2}^{2\nu}$ measurement, a total MC simulation uncertainty of 2.2 % has to be taken into account for effects related to the geometry implementation and particle tracking. It is folded into the total marginalized posterior distributions. No effect on the lower limits is observed for any of the spectral modes.

(iii) *Data acquisition and selection*
The uncertainty from data acquisition and selection is estimated to be below 0.1 % and does not alter the derived limits on $T_{1/2}^{0\nu\chi}$.

7.3 Results and discussion

Figure 3 shows the global model for the case of spectral index $n = 1$ together with the energy spectra for both the coaxial and the BEGe data sets. The p-value of the fit is 0.12. The contributions from the background contaminations, from the $2\nu\beta\beta$ decay only, and the combined spectra from the background contaminations and $2\nu\beta\beta$ decay are drawn separately. The 35868 events in the data spectrum of the golden data set were matched with 35834 events in the best-fit model for $n = 1$. Of those events, in the best fit, 54.5 are attributed to $0\nu\beta\beta\chi$ decay. For the BEGe data set, the best-fit model contains 5081.4 counts for the 5035 measured events. In this fit, 7.8 events are attributed to $0\nu\beta\beta\chi$ decay. The limit of $T_{1/2}^{0\nu\chi}$ at 90 % CI derived from the fit is also drawn (green histogram). The upper limits at 90 % CI for the remaining

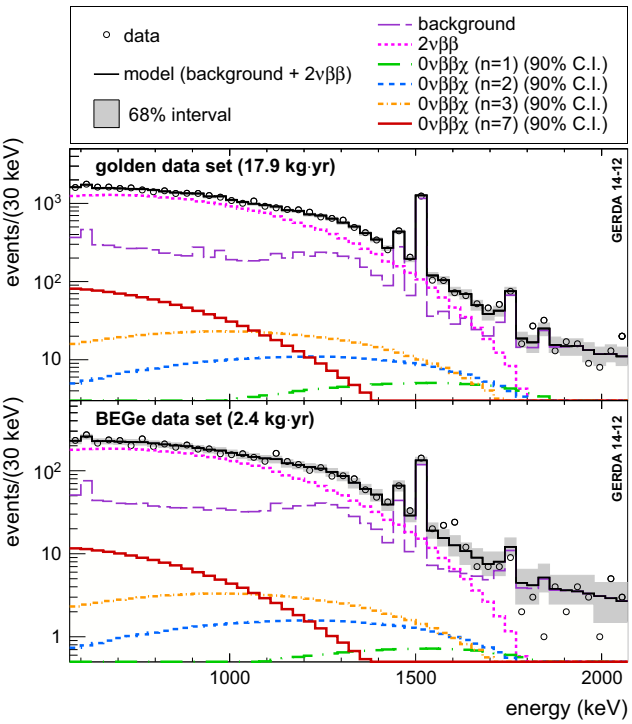

Fig. 3 Best-fit model and data energy spectrum for the coaxial and the BEGe data sets for the case of spectral index $n = 1$. The contributions from $2\nu\beta\beta$ decay and the background contributions are shown separately. The best-fit model does not contain the contributions from $0\nu\beta\beta\chi$ decay. The smallest interval of 68 % probability for the model expectation is indicated in *gray*. Also shown is the *upper limit* for $0\nu\beta\beta\chi$ decay with $n = 1$ as determined from the 90 % quantile of the marginalized posterior probability for $T_{1/2}^{0\nu\chi}$. For illustrative purpose, also the *upper limits* at 90 % CI of the other three spectral indices $n = 2, 3, 7$ are reported

three modes are reported for illustrative purpose (blue histogram for $n = 2$, orange for $n = 3$, and red for $n = 7$). The maximum of the corresponding distributions shifts to higher energy with the diminishing of the spectral index n. The resulting lower limits on $T_{1/2}^{0\nu\chi}$, determined as the 90 % quantiles of the posterior probability distributions and taking into account all uncertainties related to the fit model, are (in units of 10^{23} yr): >4.2, >1.8, >0.8 and >0.3 for $n = 1, 2, 3,$ and 7, respectively. The results are summarized in Table 3 for the different Majoron models.

The limits on $T_{1/2}^{0\nu\chi}$ presented here are the most stringent limits obtained to date for ^{76}Ge. The limits for $n = 1$ and $n = 3$ are improved by more than a factor 6 [9], the limit for $n = 7$ is improved by a factor 5 [8] compared to previous measurements. The limit for the mode with $n = 2$ is reported here for the first time.

From the lower limits on $T_{1/2}^{0\nu\chi}$, upper limits on the effective neutrino–Majoron coupling constants $\langle g \rangle$ for the models with $n = 1, 3,$ and 7 can be calculated using the following equations:

Table 3 Experimental results for the limits on $T_{1/2}^{0\nu\chi}$ of ^{76}Ge for the Majoron models given in Refs. [7,57–59]. The first half considers lepton number violating models (I) allowing $0\nu\beta\beta$ decay, while in the second half lepton number conserving models (II) are listed, where $0\nu\beta\beta$ decay is not allowed. The first column gives the model name, the second the spectral index, n, the third the information on whether one Majoron, χ, or two Majorons, $\chi\chi$, is emitted, the fourth if the Majoron is a Goldstone boson, the fifth provides its lepton number, L, the sixth the experimental limit on $T_{1/2}^{0\nu\chi}$ of ^{76}Ge obtained in this analysis. The nuclear matrix elements, $\mathcal{M}^{0\nu\chi(\chi)}$, the phase space factor, $G^{0\nu\chi(\chi)}$, and the resulting effective coupling constants, $\langle g\rangle$, are given in the seventh, eighth and ninth columns, respectively. The limits on $T_{1/2}^{0\nu\chi}$ of ^{76}Ge for the Majoron models and $\langle g\rangle$ correspond to the 90 % quantiles of the marginalized posterior probability distribution. For the case of $n = 1$, the nuclear matrix element, $\mathcal{M}^{0\nu\chi}$, from Refs. [60–66] and the phase space factor, $G^{0\nu\chi}$, from Ref. [67] are used for the calculation of $\langle g\rangle$. The given range covers the variations of $\mathcal{M}^{0\nu\chi}$ in these works. For $n = 3$ and 7, $\langle g\rangle$ is determined using the matrix elements and phase space factors from Ref. [57]. The results for $0\nu\beta\beta\chi$ ($n = 3,\ 7$) account for the uncertainty on $\mathcal{M}^{0\nu\chi(\chi)}$. For $n = 2$, only the experimental upper limit is given

Model	n	Mode	Goldstone boson	L	$T_{1/2}^{0\nu\chi}$ (10^{23} yr)	$\mathcal{M}^{0\nu\chi(\chi)}$	$G^{0\nu\chi(\chi)}$ (yr^{-1})	$\langle g\rangle$
IB	1	χ	No	0	>4.2	(2.30–5.82)	5.86×10^{-17}	$<(3.4–8.7) \times 10^{-5}$
IC	1	χ	Yes	0	>4.2	(2.30–5.82)	5.86×10^{-17}	$<(3.4–8.7) \times 10^{-5}$
ID	3	$\chi\chi$	No	0	>0.8	$10^{-3\pm1}$	6.32×10^{-19}	$<2.1^{+4.5}_{-1.4}$
IE	3	$\chi\chi$	Yes	0	>0.8	$10^{-3\pm1}$	6.32×10^{-19}	$<2.1^{+4.5}_{-1.4}$
IF	2	χ	Bulk field	0	>1.8	–	–	–
IIB	1	χ	No	−2	>4.2	(2.30–5.82)	5.86×10^{-17}	$<(3.4–8.7) \times 10^{-5}$
IIC	3	χ	Yes	−2	>0.8	0.16	2.07×10^{-19}	$<4.7 \times 10^{-2}$
IID	3	$\chi\chi$	No	−1	>0.8	$10^{-3\pm1}$	6.32×10^{-19}	$<2.1^{+4.5}_{-1.4}$
IIE	7	$\chi\chi$	Yes	−1	>0.3	$10^{-3\pm1}$	1.21×10^{-18}	$<2.2^{+4.9}_{-1.4}$
IIF	3	χ	Gauge boson	−2	>0.8	0.16	2.07×10^{-19}	$<4.7 \times 10^{-2}$

$$1/T_{1/2}^{0\nu\chi} = |\langle g\rangle|^2 \cdot G^{0\nu\chi}(Q_{\beta\beta}, Z) \cdot |M^{0\nu\chi}|^2 \quad (8)$$

and

$$1/T_{1/2}^{0\nu\chi} = |\langle g\rangle|^4 \cdot G^{0\nu\chi\chi}(Q_{\beta\beta}, Z) \cdot |M^{0\nu\chi\chi}|^2 \quad (9)$$

for single and double Majoron emission, respectively. The matrix element for the models with $n = 1$ (IB, IC and IIB) are taken from Refs. [60–66], whereas the phase space factor is that of Ref. [67]. The matrix elements for the models with $n = 3$ (ID, IE, IIC, IID, IIF) and with $n = 7$ (IIE) as well as the corresponding phase space factors are taken from Ref. [57]. The results for the upper limits on $\langle g\rangle$ are also shown in Table 3. The coupling constants allow a comparison with other isotopes. The best limits on $0\nu\beta\beta\chi$ decay of isotopes other than ^{76}Ge have been obtained for ^{100}Mo [10] and ^{136}Xe [18,19]. When comparing with the case of ^{100}Mo, it becomes obvious that the limits on $T_{1/2}^{0\nu\chi}$ determined in the present analysis are about one order of magnitude more stringent, for the case of $n = 7$ even two orders of magnitude. However, due to the differences in the matrix elements and the phase space factors, the resulting limits on $\langle g\rangle$ from ^{100}Mo and ^{76}Ge are comparable. The limits for $\langle g\rangle$ derived from ^{136}Xe are a factor of 2 to 5 more stringent due to the higher limits that had been measured for $T_{1/2}^{0\nu\chi}$.

8 Conclusions

Phase I of the GERDA experiment, located at the INFN Laboratori Nazionali del Gran Sasso (LNGS) in Italy, has been executed between November 2011 and May 2013. Utilizing the collected exposure of Phase I, an improved result of the half-life of the $2\nu\beta\beta$ process in ^{76}Ge was obtained and new limits for the half-lives of the Majoron-emitting double beta decays were produced.

The half-life for the $2\nu\beta\beta$ process is determined to be

$$T_{1/2}^{2\nu} = (1.926 \pm 0.094) \times 10^{21} \text{ yr}. \quad (10)$$

Thanks to the extremely low background level in the GERDA experiment, with a signal-to-background ratio of 3:1 in the 570–2039 keV interval and a refined background model, the measurement has an unprecedented precision (<5 %) with respect to previous experiments using ^{76}Ge. The new result is in good agreement with the one derived from a smaller data set with 5 kg yr exposure [56]. The inclusion of more components into the reference background model results in a slight increase of the best estimate for $T_{1/2}^{2\nu}$.

Majoron emission processes were searched for in the energy spectra using an exposure of 20.3 kg yr. The analysis was performed for all four possibilities of the spectral index n ($n = 1, 2, 3$, and 7). No indication for a contribution of $0\nu\beta\beta\chi$ decay was found in any of the cases. Lower limits

on the half-lives, $T_{1/2}^{0\nu\chi}$, were determined from the quantiles of 90 % probability of the marginalized posterior probability distributions. The results constitute the most stringent limits on $T_{1/2}^{0\nu\chi}$ of ^{76}Ge obtained to date. For the standard mode ($n = 1$), the lower limit is determined to be

$$T_{1/2}^{0\nu\chi} > 4.2 \times 10^{23} \text{ yr}. \quad (11)$$

From the lower limit on $T_{1/2}^{0\nu\chi}$, an upper limit on the effective neutrino–Majoron coupling constant, $\langle g \rangle$, can be inferred:

$$\langle g \rangle < (3.4 - 8.7) \times 10^{-5}. \quad (12)$$

Acknowledgments The GERDA experiment is supported financially by the German Federal Ministry for Education and Research (BMBF), the German Research Foundation (DFG) via the Excellence Cluster Universe, the Italian Istituto Nazionale di Fisica Nucleare (INFN), the Max Planck Society (MPG), the Polish National Science Centre (NCN), the Foundation for Polish Science (MPD programme), the Russian Foundation for Basic Research (RFBR), and the Swiss National Science Foundation (SNF). The institutions acknowledge also internal financial support. The GERDA Collaboration thanks the directors and the staff of the LNGS for their continuous strong support of the GERDA experiment.

Open Access This article is distributed under the terms of the Creative Commons Attribution 4.0 International License (http://creativecommons.org/licenses/by/4.0/), which permits unrestricted use, distribution, and reproduction in any medium, provided you give appropriate credit to the original author(s) and the source, provide a link to the Creative Commons license, and indicate if changes were made.
Funded by SCOAP[3].

References

1. Y. Chikashige, R.H. Mohapatra, R.D. Peccei, Phys. Rev. Lett. **45**, 1926 (1980)
2. R. Santamaria, J.W.F. Valle, Phys. Rev. Lett. **60**, 397 (1988)
3. G.B. Gelmini, M. Roncadelli, Phys. Lett. B **99**, 411 (1981)
4. The ALEPH Collaboration, The DELPHI Collaboration, The L3 Collaboration, The OPAL Collaboration, The SLD Collaboration, The LEP Electroweak Working Group, The SLD electroweak and heavy flavour groups. Phys. Rep. **427**, 257 (2006)
5. C.P. Burgess, J.M. Cline, Phys. Lett. B **298**, 141 (1993)
6. C.P. Burgess, J.M. Cline, Phys. Rev. D **49**, 5925 (1994)
7. P. Bamert, C.P. Burgess, R.N. Mohapatra, Nucl. Phys. B **449**, 25 (1995)
8. M. Günther et al., Phys. Rev. D **54**, 3641 (1996)
9. H.V. Klapdor-Kleingrothaus et al., Eur. Phys. J. A **12**, 147 (2001)
10. R. Arnold et al., Nucl. Phys. A **765**, 483 (2006)
11. R. Arnold et al., Nucl. Phys. A **678**, 341 (2000)
12. J. Argyriades et al., Phys. Rev. C **80**, 032501 (2009)
13. J. Argyriades et al., Nucl. Phys. A **847**, 168 (2010)
14. R. Arnold et al., Phys. Rev. Lett. **107**, 062504 (2011)
15. A. Barabash, V. Brudanin (NEMO-3 Collaboration), Phys. At. Nucl. **74**, 312 (2011)
16. K. Fushimi et al., Phys. Lett. B **531**, 190 (2002)
17. R. Bernabei et al., Phys. Lett. B **546**, 23 (2002)
18. A. Gando et al. (KAMLAND-Zen Collaboration), Phys. Rev. C **86**, 021601(R) (2012)
19. J.B. Albert et al. (EXO-200 Collaboration), Phys. Rev. D **90**, 092004 (2014)
20. A.S. Barabash, Phys. Rev. C **81**, 035501 (2010)
21. V.I. Tretyak, Yu. G. Zdesenko, At. Data Nucl. Data Tables **61**, 43 (1995)
22. V.I. Tretyak, Yu. G. Zdesenko, At. Data Nucl. Data Tables **80**, 83 (2002)
23. A. Gando et al. (KAMLAND-Zen Collaboration), Phys. Rev. C **85**, 0455504 (2012)
24. J.B. Albert et al. (EXO Collaboration), Phys. Rev. C **89**, 015502 (2014)
25. V.A. Rodin, A. Faessler, F. Šimkovic, P. Vogel, Nucl. Phys. A **766**, 107 (2006)
26. V.A. Rodin, A. Faessler, F. Šimkovic, P. Vogel, Nucl. Phys. A **793**, 213 (2007). (erratum)
27. F. Šimkovic, A. Faessler, V.A. Rodin, P. Vogel, J. Engel, Phys. Rev. C **77**, 045503 (2008)
28. F. Šimkovic, R. Hodak, A. Faessler, P. Vogel, Phys. Rev. C **83**, 015502 (2011)
29. E. Caurier, F. Nowacki, A. Poves, Phys. Lett. B **771**, 62 (2012)
30. J. Barea, F. Iachello, Phys. Rev. C **79**, 044301 (2009)
31. J. Suhonen, O. Civitarese, J. Phys. G Nucl. Part. Phys. **39**, 085105 (2012)
32. O. Civitarese, J. Suhonen, Nucl. Phys. A **761**, 313 (2005)
33. K.H. Ackermann et al. (Gerda Collaboration), Eur. Phys. J. C **73**, 2330 (2013)
34. M. Günther et al., Phys. Rev. D **55**, 54 (1997)
35. A. Morales, Nucl. Phys. B **77**, 335 (1999)
36. C.S. NV, Lammerdries 25, B-2439 Olen, Belgium
37. M. Agostini et al. (Gerda Collaboration), Eur. Phys. J. C. **75**, 39 (2015)
38. M. Agostini et al. (Gerda Collaboration), Eur. Phys. J. C **74**, 2764 (2014)
39. M. Agostini et al. (Gerda Collaboration), Phys. Rev. Lett. **111**, 122503 (2013)
40. M. Agostini, L. Pandola, P. Zavarise, O. Volynets, J. Instrum. **6**, P08013 (2011)
41. M. Agostini, L. Pandola, P. Zavarise, J. Phys. Conf. Ser. **368**, 012047 (2012)
42. N. Becerici-Schmidt, Results on neutrinoless double beta decay search in GERDA: background modelling and limit setting. Ph. D. thesis, Technische Universität München and Max-Planck-Institut für Physik (Werner-Heisenberg-Institut) (2014)
43. S. Hemmer, Study of lepton number conserving and non-conserving processes using GERDA Phase I data. Ph. D. thesis, Università degli Studi di Padova (2014)
44. A. Caldwell, A. Kollar, K. Kröninger, Comput. Phys. Commun. **180**, 2197 (2009)
45. M. Boswell et al., IEEE Trans. Nucl. Sci. **58**, 1212 (2011)
46. O.A. Ponkratenko, V.I. Tretyak, Yu. G. Zdesenko, Phys. At. Nucl. **63**, 1282 (2000)
47. J. Kotila, F. Iachello, Phys. Rev. C **85**, 034316 (2012)
48. M. Agostini et al. (Gerda Collaboration), Eur. Phys. J. C **73**, 2583 (2013)
49. E. Aguayo et al., Nucl. Instrum. Methods A **701**, 176 (2013)
50. S. Agostinelli et al. (GEANT Collaboration), Nucl. Instrum. Methods A **506**, 250 (2003)
51. J. Allison et al., IEEE Trans. Nucl. Sci. **53**, 270 (2006)
52. K. Amako et al., IEEE Trans. Nucl. Sci. **52**, 910 (2005)
53. E. Poon, F. Verhaegen, Med. Phys. **32**, 1696 (2005)
54. G. Cirrone et al., Nucl. Instrum. Methods A **618**, 315 (2010)
55. R. Aggarwal, A. Caldwell, Eur. Phys. J. Plus **127**, 24 (2012)
56. M. Agostini et al. (Gerda Collaboration), J. Phys. G Nucl. Part. Phys. **40**, 035110 (2013)
57. M. Hirsch, H. Klapdor-Kleingrothaus, S. Kovalenko, H. Päs, Phys. Lett. B **372**, 8 (1996)

58. C.D. Carone, Phys. Lett. B **308**, 85 (1993)
59. R.N. Mohapatra, A. Perez-Lorenzana, C.A.S. de Pires, Phys. Lett. B **491**, 143 (2000)
60. F. Šimkovic, V. Rodin, A. Faessler, O. Vogel, Phys. Rev. C **87**, 045501 (2013)
61. M.T. Mustonen, J. Engel, Phys. Rev. C **87**, 064302 (2013)
62. T.R. Rodriguez, G. Martinez-Pinedo, Phys. Rev. Lett. **105**, 252503 (2010)
63. J. Menéndez, A. Poves, E. Caurier, F. Nowacki, Nucl. Phys. A **818**, 139 (2009)
64. J. Barea, J. Kotila, F. Iachello, Phys. Rev. C **87**, 014315 (2013)
65. J. Suhonen, O. Civitarese, Nucl. Phys. A **847**, 207 (2010)
66. A. Meroni, S. Petcov, F. Šimkovic, J. High Energy Phys. **2013**, 1 (2013)
67. J. Suhonen, O. Civitarese, Phys. Rep. **300**, 123 (1998)